RESEARCH PAPER

Nitrogen Doped Graphene Quantum Dots/Manganese Dioxide Nanocomposite as Active Photocatalyst for Degradation of Crystal Violet

Seyedeh Shadi Shariati [1], Maryam Dargahi [1], Majid Masteri-Farahani [2], Abolfazl Keshtkar Vanashi [1]*

[1] *Department of Chemistry, Faculty of Science, Imam Khomeini International University, Qazvin, Islamic Republic of Iran*

[2] *Faculty of Chemistry, Kharazmi University, Tehran, Islamic Republic of Iran*

ARTICLE INFO

Article History:
Received 06 June 2025
Accepted 24 September 2025
Published 01 October 2025

Keywords:
Crystal violet
Manganese dioxide
Nanocomposite
Photocatalyst
Quantum dot

ABSTRACT

In this research, nitrogen doped graphene quantum dots (N-GQD) were synthesized by hydrothermal method and used to prepare novel nanocomposite with manganese dioxide (MnO_2/N-GQD). The products were characterized by Fourier-transform infrared (FT-IR), UV-Vis spectroscopy, energy-dispersive X-ray analysis (EDX), X-ray diffraction (XRD), scanning electron microscopy (SEM). The photocatalytic activities of N-GQD and MnO_2/N-GQD were investigated in the photodegradation of crystal violet under visible light as well as ultraviolet irradiation in short time intervals. The effect of various parameters such as initial dye concentration, amount of photocatalyst, pH, and temperature on the efficiency of the dye removal was also examined and optimal condition was determined. The results showed that the photodegradation process is fast and highly efficient. The equilibrium time is about 5-40 min depending on the amount of photocatalyst and initial dye concentration, and efficiency is 100%. Finally, kinetic studies of reaction showed that the kinetics of reaction follows the first-order model.

How to cite this article
Shariati S., Dargahi M., Masteri-Farahani M., Keshtkar Vanashi A. Nitrogen Doped Graphene Quantum Dots/Manganese Dioxide Nanocomposite as Active Photocatalyst for Degradation of Crystal Violet. J Nanostruct, 2025; 15(4):1875-1887. DOI: 10.22052/JNS.2025.04.035

INTRODUCTION

Over the past decades, pollutants have been important challenges in environmental problems. Therefore, many researchers have been encouraged to provide solutions for air, water, and environmental pollution [1–4]. Industrial wastewater pollutants are one of the biggest problems in the world as it endangers life [5–7]. Synthetic dyes have been used in various industries such as cosmetics, dyeing, plastics, textile, and stationery [8,9]. For example, crystal violet as a cationic dye has been greatly applied in the textile industry. However, it has carcinogenic and mutagenic effects and may cause serious health problems [10]. Therefore, these dyes cause pollution of water and nature and their removal from industrial wastewater is crucial. Many techniques and methods have been suggested for dye removal from aqueous solutions such as physical adsorption, oxidation, biological methods, electrochemistry, membrane separation, filtration, and photocatalytic degradation [11–17]. Among them, photocatalytic reactions play a major role in pollution removal

* *Corresponding Author Email: dargahi@sci.ikiu.ac.ir*

and in various compounds and composites have been developed for this purpose[15,16,18–21]. The nanostructured photocatalysts, especially, quantum dots (QDs) have attracted great attention because of their unique properties [1,22–24]. The QDs are semiconductor nanostructures with discrete quantized energy levels which can absorb electromagnetic irradiations and then emit them with high efficiency. The difference between energy levels inversely depends on the size of QDs and thus their emission can be seen in different colors depending on their size [25–29].

Graphene quantum dots (GQDs) consist of carbon (sp^2 and sp^3) and oxygen in the form of various functional groups. The GQDs have strong luminescence, conductivity, biocompatibility, and high solubility which make them useful in drug delivery, bio-imaging, catalytic systems, photovoltaic devices, solar cells, etc. [30–38]. The incorporation of hetero-atoms such as nitrogen in the structure of GQD gives it amended properties [39,40]. For instance, Palladium nanoparticles supported on N-GQD have been used as catalyst for oxygen reduction [41]. B-GQD and N-GQD as hybrid nanoplatelets have been used as efficient electrocatalysts for oxygen reduction [42]. Also, N-GQD itself has been used as a catalyst for oxygen reduction [32,43]. Moreover, composites of GQDs were synthesized and applied for various applications such as sensors, supercapacitors, photocatalysis, solar cell, adsorption, and antimicrobial activity [36 – 46]. Photocatalytic dye degradations have been done by various QDs as efficient photocatalysts [25]. Ding et al. reported degradation of rhodamine B (RhB), methyl orange (MO), and methylene blue (MB) by ZnO foam/carbon quantum dots nanocomposite as a photocatalyst under UV and visible light irradiation [55]. Photodegradation of methyl orange under visible light irradiation by CdS QDs/ chitosan composite films was also reported [56]. Safardoust-Hojaghan et al. synthesized N-GQD/ TiO_2 and used it in the degradation of methylene blue [57]. Moreover, GQD/TiO_2 composite has been used for the photodegradation of dye [14]. In our previous work, CdS quantum dot nanocomposite hydrogels (QD-NCH) were synthesized by in situ copolymerization cross-linking method using acrylic acid and κ-carrageenan and was applied for the adsorption of cationic dyes, crystal violet (CV) and malachite green (MG) [25].

In this work, N-GQD has been prepared by hydrothermal method and characterized by some analyses. Then, it was used for the photodegradation of CV under visible and UV irradiations. As the results were not satisfactory, MnO_2/N-GQD nanocomposite was synthesized and applied for CV photodegradation under visible and UV irradiations. The results showed that the photodegradation process is fast and highly efficient. The equilibrium time is about 5-40 min depending on the amount of photocatalyst and initial dye concentration, and efficiency is 100%.

MATERIALS AND METHODS

Materials and instruments

Crystalline citric acid ($C_6H_8O_7$), Urea (CH_4N_2O), manganese dioxide (MnO_2), sodium hydroxide, and hydrochloric acid were prepared from Merck (Germany), crystal violet ($C_{25}N_3H_{30}Cl$) was purchased from Sigma Aldrich (USA), and ethanol was prepared from Bidestan Company (Iran). All of the materials were used without further purification.

Absorbance measurements were employed using UV–Vis Photonix Ar 2015 spectrophotometer (Iran). FT-IR spectra of the samples in the form of KBr pellets were recorded using a Tensor 27, Bruker FT-IR spectrophotometer (Germany). The surface morphology of the samples was investigated using a field emission scanning electron microscope FESEM Mira III with SAMX detector (Czech Republic). X-ray diffraction analysis of samples was obtained using PW1730 (Netherland).

Preparation of Nitrogen doped graphene quantum dot (N-GQD)

A solution of crystalline citric acid (0.21 g) and urea (0.18 g) in 5 ml of deionized water was transferred into a 25 ml Teflon lined stainless steel autoclave and placed in the oven at 170 °C for 4 hours. After cooling, 40 ml of ethanol was added to the resulting mixture and centrifuged for 20-30 min with 8000 rpm. The precipitate was separated, washed with ethanol several times, centrifuged, and finally dried at room temperature.

Preparation of MnO_2/N-GQD nanocomposite

To prepare MnO_2/N-GQD nanocomposite, 15 mg of N-GQD was dispersed in 15 ml of deionized water and stirred for 30 min. Afterward, 50 mg of MnO_2 powder was added and the mixture was stirred for 4 hours. Then, the mixture was transferred into the Teflon lined stainless steel

autoclave and was heated to 110 °C for 2 hours. Finally, 40 ml of ethanol was added to the sample and the precipitate was separated with centrifugation.

Evaluation of the photocatalytic activity of the MnO_2/N-GQD

To investigate the photocatalytic activity of MnO_2/N-GQD nanocomposite, dye degradation was carried out under UV and visible irradiation in the presence of MnO_2/N-GQD nanocomposite as photocatalyst. First, a solution containing 50 ml of crystal violet (10 ppm) was prepared and then 0.05 g of MnO_2/N-GQD was added to the solution. The solution was placed in dark or in the presence of visible light (200-watt tungsten bulb) as well as ultraviolet light (Mercury lamp 125 W) at a distance of 20 cm from the solution upon stirring. After certain times, 3 ml of the solution was taken and centrifuged to separate the nanocomposite. The residual dye concentration was determined using UV-Vis absorption spectroscopy at λ_{max} = 590 nm. It should be noted that the experiment was also performed by N-GQD and MnO_2 and the results were compared with MnO_2/N-GQD nanocomposite.

Investigation of the effect of various parameters on the photocatalytic dye degradation

To study the effect of pH on the photocatalytic dye degradation, dye solutions with various pH values from 2 to 10 were prepared by adding hydrochloric acid or sodium hydroxide solutions. To evaluate the effect of contact time on photocatalytic dye degradation, the absorption of dye solution was measured at certain times by UV-Vis spectroscopy. To investigate the effect of photocatalyst amount on the photocatalytic dye degradation, dye solutions with initial concentration of 10 ppm were prepared. Then, determined amount of the MnO_2/N-GQD nanocomposite (m= 0.005 g to 0.1 g) was added to the solutions, separately. To examine the effect of initial dye concentration on the photocatalytic dye degradation, dye solutions with concentration of 5-50 ppm were prepared, and then 0.05 g of the MnO_2/N-GQD was added to each solution. After the equilibrium is established, the residue of dye concentration was determined. To study the effect of temperature, 50 ml of CV solution (C_0=10 ppm)

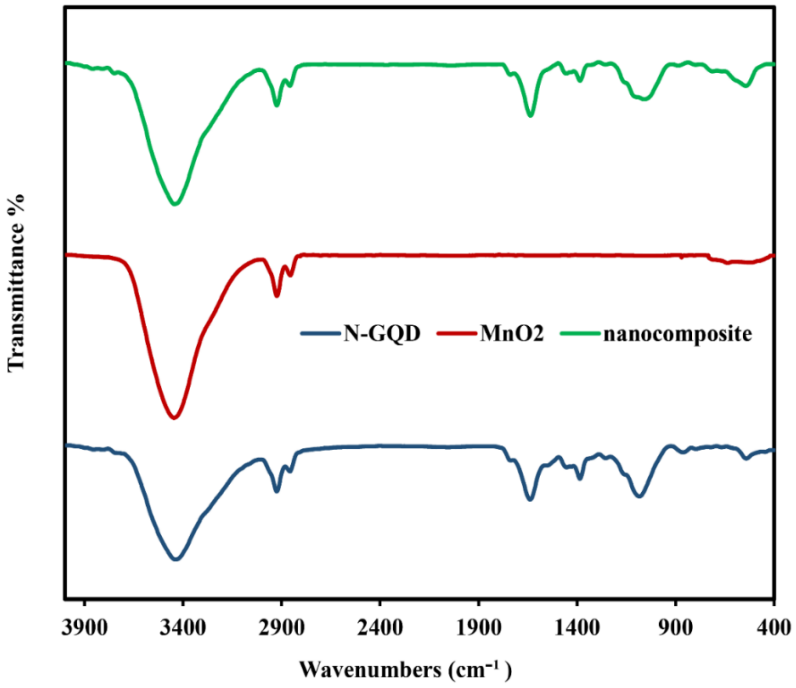

Fig. 1. FT-IR spectra of N-GQD, MnO_2, and MnO_2/N-GQD nanocomposite.

was prepared and, 0.05 g of the MnO_2/N-GQD was added to the solution (at pH= 5.5) and heated to 35, 40, 45, 50, 55 and, 60 °C and cooled by an ice bath for 20 °C.

The percent of degradation of dye was calculated by the following equation:

$$D\% = \frac{C_0 - C_e}{C_0} \times 100 \quad (1)$$

where, C_0 (mg. L^{-1}) and C_e (mg. L^{-1}) are initial and equilibrium dye concentrations, respectively.

RESULTS AND DISCUSSION

Characterization of N-GQD and MnO_2/ N-GQD nanocomposite

The FT-IR spectra of N-GQD, MnO_2, and MnO_2/ N-GQD nanocomposite are shown in Fig. 1. As can be seen, the characteristic bands of N-GQD are observed at about 3450 cm^{-1} (stretching vibration of OH), 2930 cm^{-1} (stretching vibration of C-H), 1705 cm^{-1} (stretching vibration of C=O), 1636 cm^{-1} (bending of NH), and 1080 cm^{-1} (stretching vibration of C-O-C). The bands of MnO_2 were appeared at 521 cm^{-1} attributed to Mn-O stretching vibration and 3450 cm^{-1} due to O-H stretching of associated H_2O. FT-IR spectrum of MnO_2/N-GQD nanocomposite exhibits all of the bands of N-GQD and MnO_2, confirming the formation of nanocomposite.

X-ray diffraction (XRD) pattern of N-GQD (Fig. 2) indicates a broad peak with a maximum at about θ = 27° indicating its weak crystalline structure. On the other hand, in the XRD pattern of nanocomposite, the sharp peaks which are consistent with the standard data (PDF#00-024-0735) indicate the presence of crystalline MnO_2 in the nanocomposite.

Chemical composition of the N-GQD and MnO_2/ N-GQD nanocomposite were investigated by

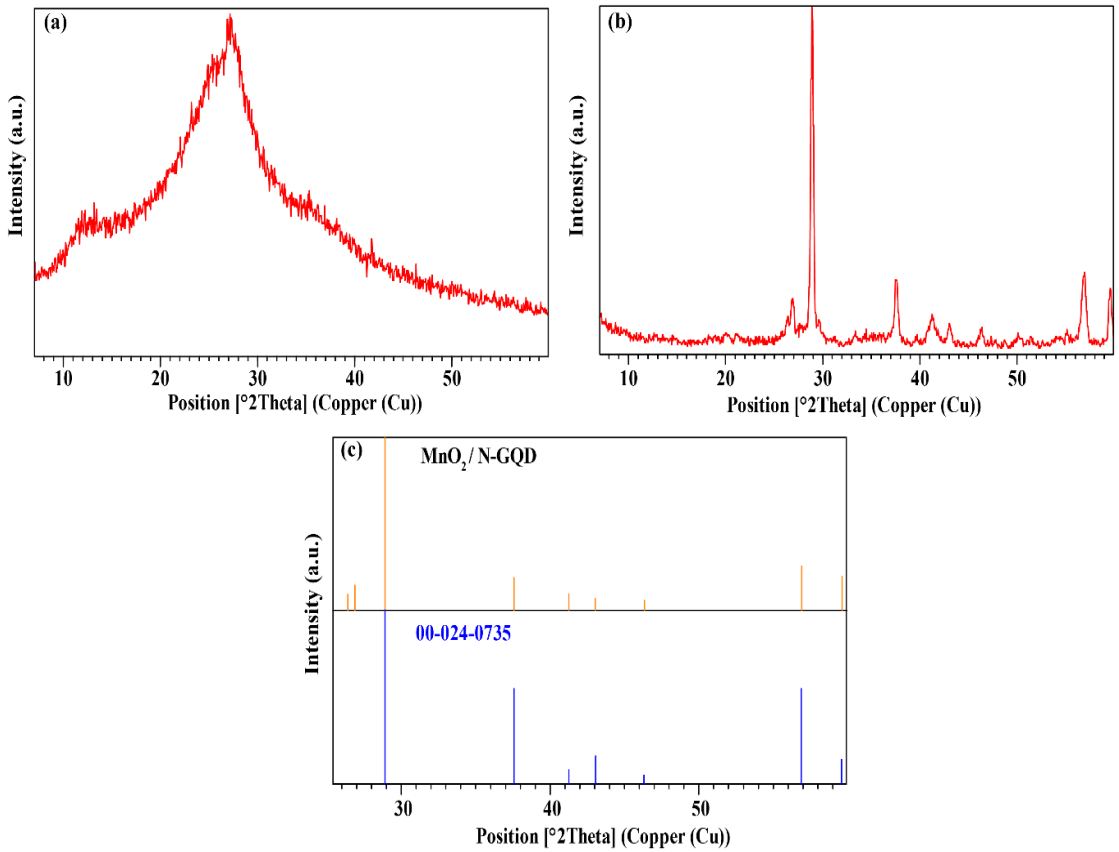

Fig. 2. XRD patterns of N-GQD (a) and MnO_2/N-GQD (b), Comparison of MnO_2/N-GQD peaks with standard XRD pattern of MnO_2 (PDF#00-024-0735) (c).

energy-dispersive X-ray (EDX) analysis. As can be seen in Fig. 3, the EDX spectra of the N-GQD and MnO_2/N-GQD show characteristic peaks of carbon, oxygen, and nitrogen in the N-GQD structure and carbon, oxygen, nitrogen, and manganese in the MnO_2/N-GQD nanocomposite. The surface morphology of the nanocomposite is shown in the SEM image and elemental distribution over the MnO_2/N-GQD can be seen in the mapping image of the nanocomposite (Fig. 2).

In the UV-Vis absorption spectrum of the N-GQD (Fig. 4), three major bands can be seen at 230, 345, and 395 nm attributed to the π → π* transition of the C sp^2 domains, n → π* transition of C=O bonds, n → π* transition of C=N, respectively. In the UV-Vis absorption spectrum of the MnO_2/N-GQD nanocomposite, the absorption bands of N-GQD are observed again and a new peak at about 430 nm is appeared due to the presence of MnO_2 component. The band gap of the N-GQD was calculated by Tauc equation:

$$\alpha h\nu = A(h\nu - E_g)^n \quad (2)$$

where, α, hν, E_g, A, and n are absorption coefficient, the photon energy, band gap, a proportional constant, and an exponent which equals 1/2 for direct transitions and 2 for indirect transitions [58]. The E_g of the N-GQD is obtained

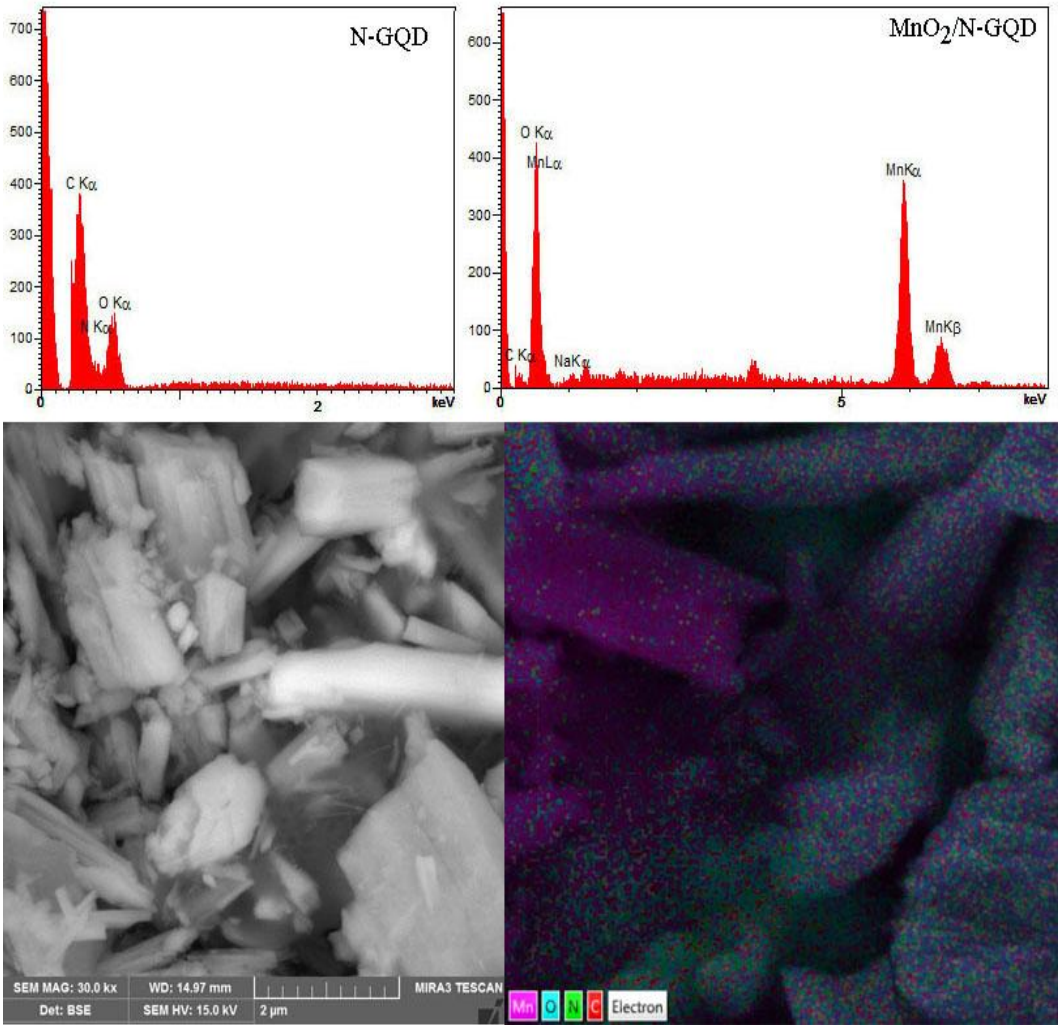

Fig. 3. EDX analysis of N-GQD and MnO_2/N-GQD (top), SEM and mapping image of MnO_2/N-GQD (bottom).

as 2.6 eV which is according to the band gap of the N-GQD reported between 2.2 to 3.4 in the previous researches [33].

Comparison between various conditions for degradation (or removal) of dye solution

As can be seen in Fig. 5a, the dye degradation in the absence of catalyst showed a poor efficiency (about 2% at dark, 8% at UV light, and 10% at visible light). The results confirm that the catalyst has an important role in this reaction. Figs 5b-d also show a comparison between three catalysts i.e. MnO_2, N-GQD, and MnO_2/N-GQD nanocomposite in the dye degradation. In the given conditions, degradation (or adsorption) of dye in the presence of N-GQD has the lowest efficiency while in the presence of nanocomposite the maximum efficiency has been reached. The comparison of three catalysts at dark (Fig. 5d) confirms that the dye degradation is progressed through the photocatalytic process. Also, it can be concluded that the small part of dye removal is related to the adsorption on the catalyst as adsorbent. As can be seen in all graphs, the equilibrium time for the processes can be determined.

The effect of the various parameters on the photocatalytic degradation of dye

The effect of various parameters such as initial dye concentration, amount of photocatalyst, pH, and temperature on the photocatalytic degradation of dye were investigated and the results were shown in Fig. 6.

The effect of initial concentration

The percentage of photocatalytic degradation of CV decreased with an increase of initial CV concentration (Fig. 6a), which is due to the decreased surface of photocatalyst compared to dye molecules. It can be noted, the percentage of dye degradation was increased over time at higher concentration, indeed, equilibrium time increased with increasing of dye concentration.

The effect of dose of photocatalyst

With increasing the dose of photocatalyst, the number of available active sites increases which leads to an increased dye degradation percent and also increases the rate of degradation (Fig. 6b). This means that the equilibrium times are shorter at a higher amount of photocatalyst (Table. 1).

The effect of pH

The CV is sensitive to pH, this means that the structure of CV changes in acidic and basic pH, so the best pH for investigation of photocatalytic degradation is the neutral pH (5.5-7.5). In acidic pH, the maximum wavelength of UV absorption was changed and in basic pH, CV was degraded by hydroxyl groups without any catalyst (Fig. 6c).

The effect of temperature

The results show that the higher temperature leads to the higher photocatalytic degradation of CV (Fig. 6d). On the other hand, the rate of photodegradation increases with the increased temperature.

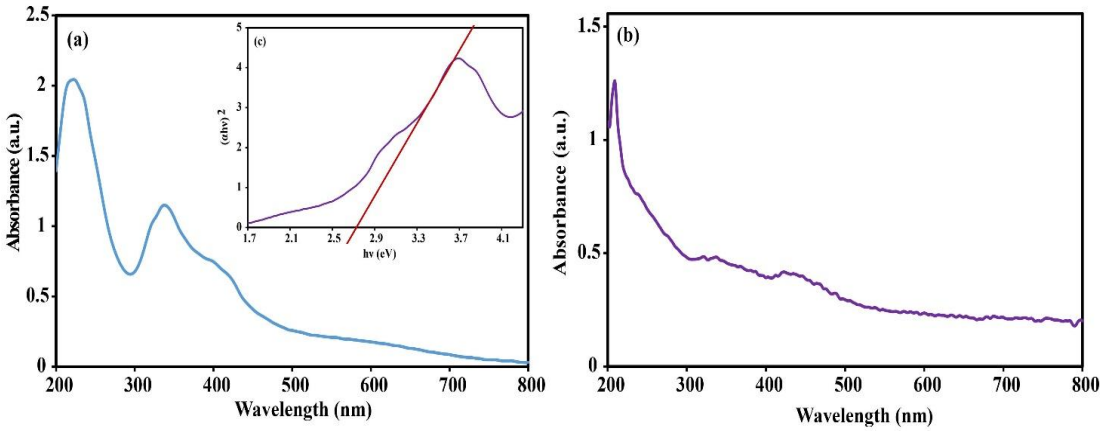

Fig. 4. UV absorption spectra of N-GQD, and MnO_2/N-GQD, inset shows the Tauc plot of N-GQD

Contact time of degradation of CV by MnO_2/N-GQD nanocomposite

Fig. 7d confirms the effect of contact time on the activity of catalyst. In other words, this parameter determined the time of the end of reactions. As can be seen, the photocatalytic decolorization of CV solution increases remarkably up to 40 min under visible light and 55 min under UV irradiation, and then no significant change can be observed with irradiation time.

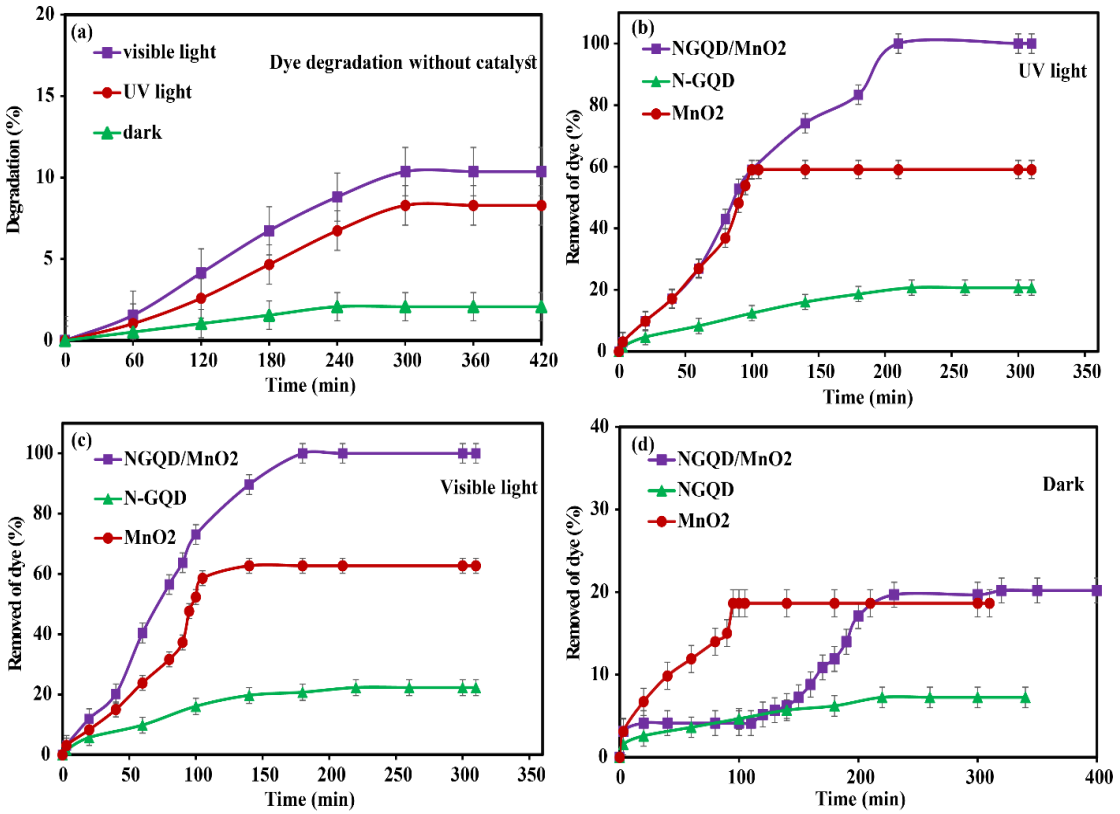

Fig. 5. Comparison between various conditions for degradation or removal of crystal violet from solution, (a) dye degradation without catalyst, (b) dye degradation in the presence of three catalysts under visible light, (c) dye degradation in the presence of three catalysts under UV light, (d) dye degradation in the presence of three catalysts at dark condition.

Table 1. The effect of the amount of photocatalyst on the equilibrium time (removal of dye 100%, C_0= 10 ppm, T= 27°C, pH= 5.5).

Amount of MnO_2/N-GQD (g)	Equilibrium time under UV (min)	Equilibrium time under visible (min)
0.01	105	90
0.03	80	60
0.05	55	40
0.08	20	15
0.1	10	5

The kinetic study of photocatalytic degradation of CV

Kinetic studies aiming to determine the mechanism of processes are one of the valuable parts of researches. In this work, to investigate the kinetics of photocatalytic degradation of CV, three kinetic models were used and the experimental data were fitted by them. These models are the zero-order model, the first-order model, and the second-order model.

The zero-order kinetic model describe the rate of reactions independent of the concentration of reactants [59]. This means that the rate of the reaction is equal to the rate constant, k_0, of that reaction. The differential form of the zeroth-order rate law is shown as the following equation:

$$\text{rate} = -\frac{dC_t}{dt} = k_0 {C_t}^0 = k_0 = \text{constant} \quad (3)$$

and, the integrated form of this model:

$$\int_{C_0}^{C_t} dC_t = -\int_0^t k_0 \, dt \quad (4)$$

$$C_t = -k_0 \, t + C_0 \quad (5)$$

where, C_t and C_0 are reactant concentration at time t and initial reactant concentration, respectively, t shows time, and k_0 is a rate constant. So, if the diagram of C_t versus time is plotted and this diagram is linear (the experimental data follows linear equation (5)), it can be said that the rate of reaction obeys the zero-order model [60]. Fig. 7a shows the fitting plot of the zero-order model.

In the first-order rate law, the rate of reaction is linearly proportional to the reactant concentration. The differential equation describing first-order

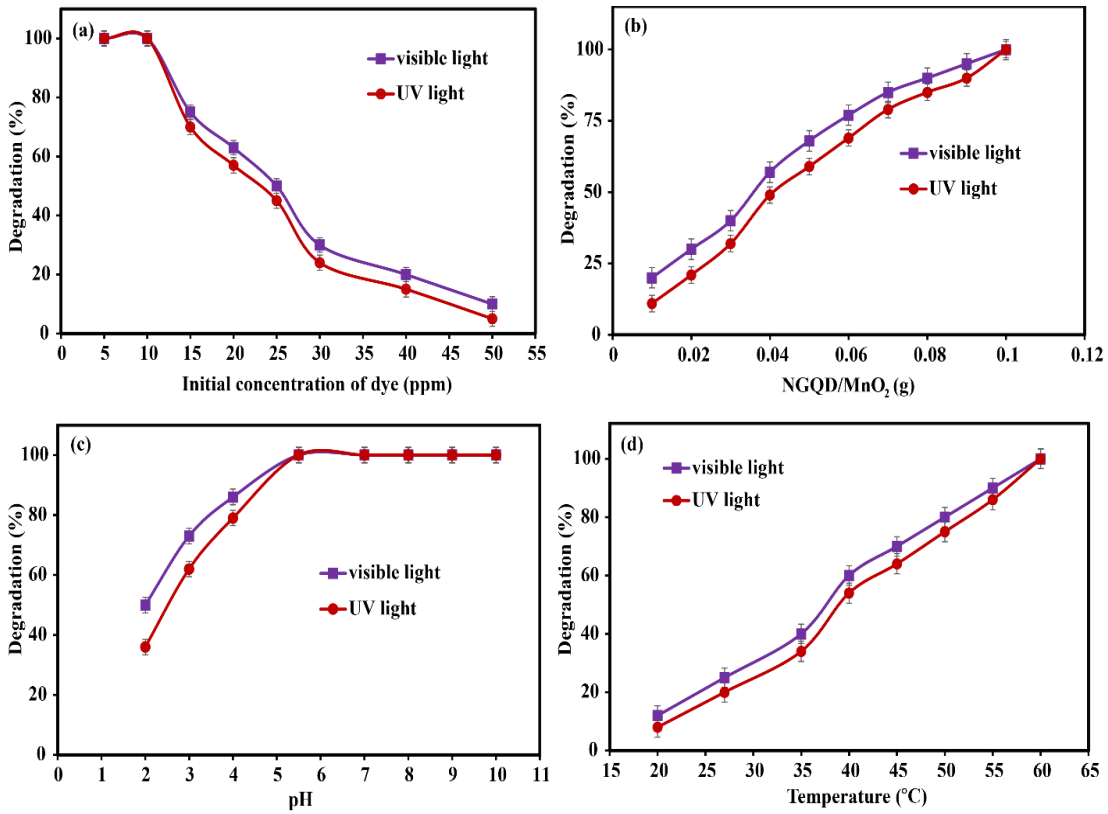

Fig. 6. The effect of initial concentration of CV solution (a), the amount of photocatalyst (b), pH (c), and temperature (d) on the photocatalytic degradation of CV.

kinetics is given below:

$$\text{rate} = -\frac{dC_t}{dt} = k_1 C_t \quad (6)$$

and, the integral representation:

$$\int_{C_0}^{C_t} \frac{dC_t}{C_t} = -\int_0^t k_1 dt \quad (7)$$

$$\ln C_t = -k_1 t + \ln C_0 \quad (8)$$

where, k_1 is a rate constant. The plot of ln C_t versus time is linear in this model. In other words, to test if the reaction is a first-order reaction, plot the natural logarithm of a reactant concentration versus time. If the graph is linear and has a negative slope, the reaction must be a first-order reaction. Fig. 7b shows the fitting diagram of the first-order model.

In the reactions that follow the second-order rate low, the relation between the inverse of reactant concentration and time is linear[61]. The differential rate law for the simplest second-order reaction in which 2A → products is as follows:

$$\text{rate} = -\frac{dC_t}{dt} = k_2 {C_t}^2 \quad (9)$$

the integrated form of this model:

$$\frac{1}{C_t} = \frac{1}{C_0} + k_2 t \quad (10)$$

where, k_2 is a rate constant. In this model, the graph of $1/C_t$ versus time is linear. Fig. 7c shows the fitting diagram of the second-order kinetic model. As can be seen, the first-order model has the best

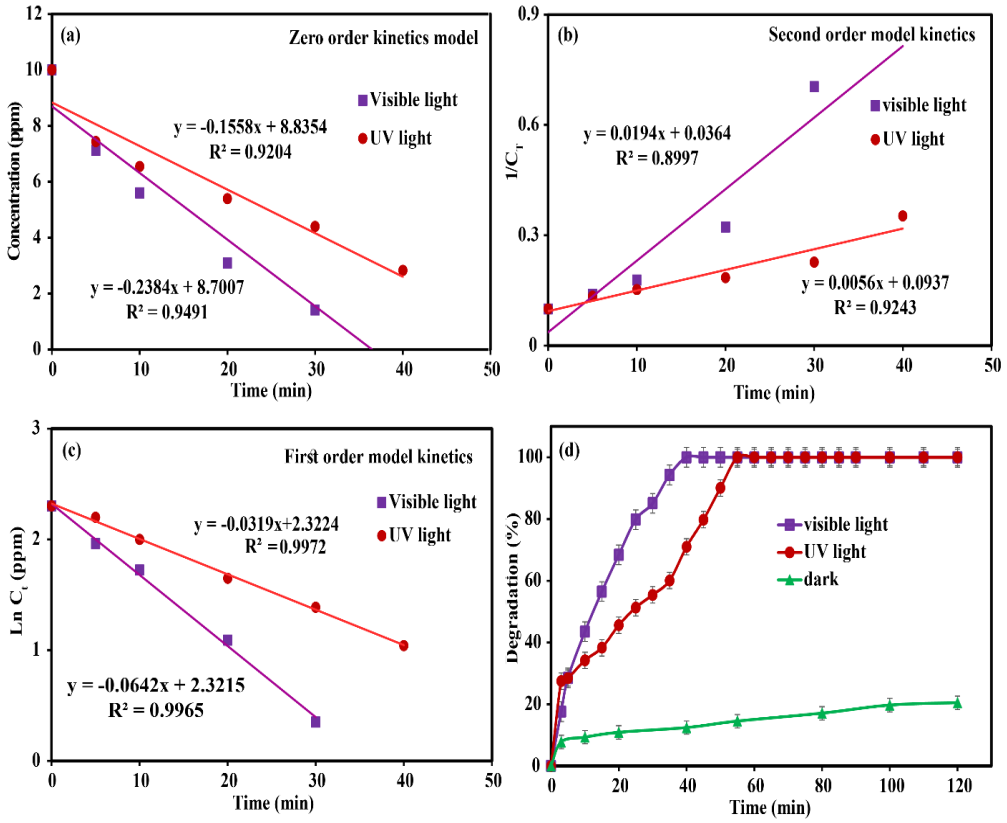

Fig. 7. Diagrams of zero-order kinetic model (a) first-order kinetic model (b) second-order kinetic model (c) and contact time effect of dye degradation by nanocomposite (d).

correlation coefficient comparison among two other models, it can be concluded that the rate of photocatalytic degradation of CV by synthesized photocatalyst (MnO_2/N-GQD nanocomposite) follows the first-order kinetic model. The rate constants and R^2 of the three models are shown in Table 2.it should be noted that the data for fittings was from the start of degradation to equilibrium time.

Photocatalytic mechanism

The mechanism of CV photocatalytic degradation process over MnO_2/N-GQD nanocomposites is proposed in Fig. 8. Under UV or visible irradiated light, the electron of MnO_2 is transferred from the valence band to the conduction band to form a hole. Holes reacted with hydroxyl ions to produce hydroxyl radicals[62]. On the other hand, transferred electrons reacted with oxygen molecules to produce superoxide radicals. These radicals can directly result in the mineralization of CV into CO_2 and H_2O or indirectly degrade the CV by forming other active species[63]. The N-GQD enhance light-driven photodegradation by allowing the excited electrons to be prevented from recombination[64]. As shown in Fig. 5, photocatalytic performance is highly enhanced by 1.6 times.

CONCLUSION

The synthesis of N-GQDs and MnO_2/N-GQD nanocomposite was successfully done and the characterization techniques such as FT-IR spectroscopy, XRD, EDX, Map analysis, SEM, UV-Vis spectroscopy, and PL analysis confirmed their synthesis and their structures. Then, MnO_2/N-GQD as a photocatalyst was used to degradation of CV from aqueous solutions. The results show

Table 2. Kinetic parameters of dye degradation reaction by photocatalyst MnO_2/ N-GQD.

Kinetic models	Kinetic constant & R squared value	Visible light	UV light
Zero order	k_0 (g. ml^{-1}. min^{-1})	0.2384	0.1558
	R^2	0.9491	0.9204
First order	k_1(min^{-1})	0.0642	0.0319
	R^2	0.9965	0.9972
Second order	k_2 (g^{-1}. ml. min^{-1})	0.0194	0.0056
	R^2	0.8997	0.9243

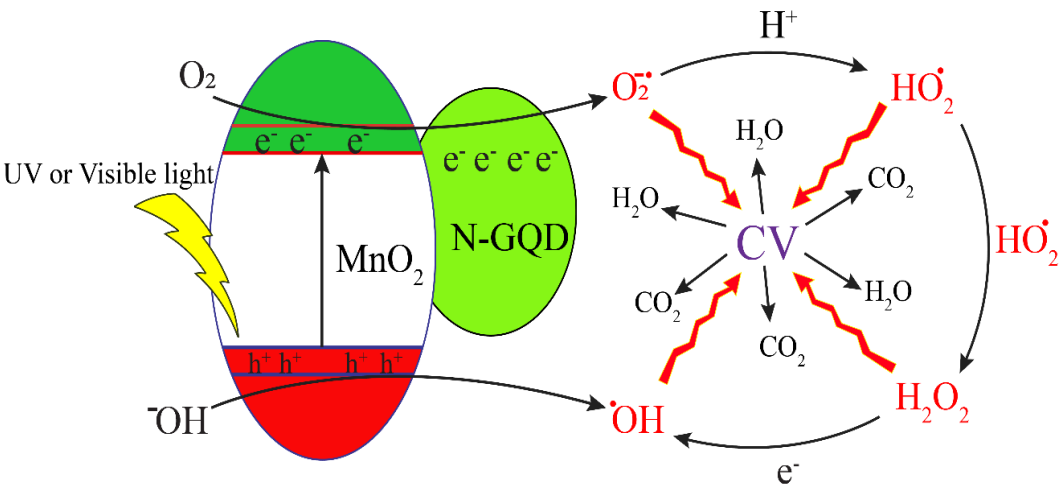

Fig. 8. Schematic of proposed photodegradation mechanism of CV in the presence of MnO_2/N-GQD.

that the photocatalyst has excellent performance under visible light as well as UV irradiation in a very short time (≈ 10 min) has an efficiency of 100%. The experiments confirm that the nanocomposite has excellent photocatalytic activity in comparison with individual N-GQD and MnO_2. The kinetic study of the reaction depicts that this photocatalytic degradation obeys the first-order model.

ACKNOWLEDGMENT

The authors are thankful to Imam Khomeini International University for the financial support of this study.

CONFLICT OF INTEREST

The authors declare that there is no conflict of interests regarding the publication of this manuscript.

REFERENCES

1. Shanmugam M, Alsalme A, Alghamdi A, Jayavel R. Enhanced Photocatalytic Performance of the Graphene-V_2O_5 Nanocomposite in the Degradation of Methylene Blue Dye under Direct Sunlight. ACS Applied Materials and Interfaces. 2015;7(27):14905-14911.
2. Liu F, Leung YH, Djurišić AB, Ng AMC, Chan WK. Native Defects in ZnO: Effect on Dye Adsorption and Photocatalytic Degradation. The Journal of Physical Chemistry C. 2013;117(23):12218-12228.
3. Dargahi M, Ghasemzadeh H, Bakhtiary A. Highly efficient absorption of cationic dyes by nano composite hydrogels based on κ-carrageenan and nano silver chloride. Carbohydr Polym. 2018;181:587-595.
4. Gupta VK, Kumar R, Nayak A, Saleh TA, Barakat MA. Adsorptive removal of dyes from aqueous solution onto carbon nanotubes: A review. Advances in Colloid and Interface Science. 2013;193-194:24-34.
5. Wan Ngah WS, Teong LC, Hanafiah MAKM. Adsorption of dyes and heavy metal ions by chitosan composites: A review. Carbohydr Polym. 2011;83(4):1446-1456.
6. Gupta VK, Ali I, Saini VK. Defluoridation of wastewaters using waste carbon slurry. Water Res. 2007;41(15):3307-3316.
7. Wang X, Liu Z, Ye X, Hu K, Zhong H, Yu J, et al. A facile one-step approach to functionalized graphene oxide-based hydrogels used as effective adsorbents toward anionic dyes. Appl Surf Sci. 2014;308:82-90.
8. Bansal P, Chaudhary GR, Mehta SK. Comparative study of catalytic activity of ZrO_2 nanoparticles for sonocatalytic and photocatalytic degradation of cationic and anionic dyes. Chem Eng J. 2015;280:475-485.
9. Liu X, Zhang T, Xu D, Zhang L. Microwave-Assisted Catalytic Degradation of Crystal Violet with Barium Ferrite Nanomaterial. Industrial and Engineering Chemistry Research. 2016;55(46):11869-11877.
10. Sarma GK, Sen Gupta S, Bhattacharyya KG. Adsorption of Crystal violet on raw and acid-treated montmorillonite, K10, in aqueous suspension. J Environ Manage. 2016;171:1-10.
11. Zangeneh H, Zinatizadeh AAL, Habibi M, Akia M, Hasnain Isa M. Photocatalytic oxidation of organic dyes and pollutants in wastewater using different modified titanium dioxides: A comparative review. Journal of Industrial and Engineering Chemistry. 2015;26:1-36.
12. Han H, Wei W, Jiang Z, Lu J, Zhu J, Xie J. Removal of cationic dyes from aqueous solution by adsorption onto hydrophobic/hydrophilic silica aerogel. Colloids Surf Physicochem Eng Aspects. 2016;509:539-549.
13. Sun X, Zhang J, Fu Z. Polyoxometalate Cluster Sensitized with Copper-Viologen Framework for Efficient Degradation of Organic Dye in Ultraviolet, Visible, and Near-Infrared Light. ACS Applied Materials and Interfaces. 2018;10(42):35671-35675.
14. Pan D, Jiao J, Li Z, Guo Y, Feng C, Liu Y, et al. Efficient Separation of Electron–Hole Pairs in Graphene Quantum Dots by TiO_2 Heterojunctions for Dye Degradation. ACS Sustainable Chemistry and Engineering. 2015;3(10):2405-2413.
15. Dargahi M, Masteri-Farahani M, Shahsavarifar S, Feizi M. Microemulsion-mediated preparation of $Ce2(MoO_4)_3$ nanoparticles for photocatalytic degradation of crystal violet in aqueous solution. Environmental Science and Pollution Research. 2020;27(11):12047-12054.
16. Mohammadikish M, Yarahmadi S, Molla F. A new water-insoluble coordination polymer as efficient dye adsorbent and olefin epoxidation catalyst. J Environ Manage. 2020;254:109784.
17. Mohammadikish M, Jahanshiri D. Rapid adsorption of cationic and anionic dyes from aqueous solution via metal-based coordination polymers nanoparticles. Solid State Sciences. 2020;99:106063.
18. Mohammadikish M, Zaeemdar B. Synthesis of Fe_3O_4@Zn-BDC nanocomposite for the removal of MB from aqueous solution. Colloid and Interface Science Communications. 2021;45:100529.
19. Yaqoubi M, Salavati-Niasari M, Ghanbari M. S-Scheme $CuMn_2O_4$/g-C_3N_4 heterojunction: fabrication, characterization, and investigation of photodegradation potential of organic pollutants. Applied Water Science. 2024;15(1).
20. Yousefzadeh F, Salavati-Niasari M, Ghanbari M. Visible light photocatalytic degradation of water-soluble organic pollutants in aqueous solution by thulium copper oxide nanostructures: sonochemical synthesis, characterization, optimization of conditions, and mechanisms. Applied Water Science. 2025;15(2).
21. Hosseini M, Ghanbari M, Mahdi MA, Almaamori MH, Alhassan ZAA, Salavati-Niasari M. Dicobalt orthosilicate-graphitic carbon nitride nanocomposites as promising visible-light nanocatalysts for removal of water-soluble organic dyes. Applied Water Science. 2025;15(2).
22. Kuvarega AT, Krause RWM, Mamba BB. Nitrogen/Palladium-Codoped TiO_2 for Efficient Visible Light Photocatalytic Dye Degradation. The Journal of Physical Chemistry C. 2011;115(45):22110-22120.
23. Najafi M, Abbasi A, Masteri-Farahani M, Janczak J. Sonochemical preparation of bimetallic (Cu/Mo) oxide nanoparticles as catalysts for dye degradation under mild conditions. Polyhedron. 2015;93:76-83.
24. Najafi M, Abbasi A, Masteri-Farahani M, Janczak J. Two novel octamolybdate nanoclusters as catalysts for dye degradation by air under room conditions. Dalton Transactions. 2015;44(13):6089-6097.

25. Dargahi M, Ghasemzadeh H, Torkaman A. CdS quantum dot nanocomposite hydrogels based on κ-carrageenan and poly (acrylic acid), photocatalytic activity and dye adsorption behavior. Polym Bull. 2018;76(10):5039-5058.
26. Bardajee GR, Hooshyar Z. Optical properties of water soluble CdSe quantum dots modified by a novel biopolymer based on sodium alginate. Spectrochimica Acta Part A: Molecular and Biomolecular Spectroscopy. 2013;114:622-626.
27. Zhou W, Coleman JJ. Semiconductor quantum dots. Curr Opin Solid State Mater Sci. 2016;20(6):352-360.
28. Costas-Mora I, Romero V, Lavilla I, Bendicho C. An overview of recent advances in the application of quantum dots as luminescent probes to inorganic-trace analysis. TrAC, Trends Anal Chem. 2014;57:64-72.
29. Shen L-M, Liu J. New development in carbon quantum dots technical applications. Talanta. 2016;156-157:245-256.
30. Kumar S, Aziz SKT, Girshevitz O, Nessim GD. One-Step Synthesis of N-Doped Graphene Quantum Dots from Chitosan as a Sole Precursor Using Chemical Vapor Deposition. The Journal of Physical Chemistry C. 2018;122(4):2343-2349.
31. Liu Z, Robinson JT, Sun X, Dai H. PEGylated Nanographene Oxide for Delivery of Water-Insoluble Cancer Drugs. Journal of the American Chemical Society. 2008;130(33):10876-10877.
32. Li Q, Zhang S, Dai L, Li L-s. Nitrogen-Doped Colloidal Graphene Quantum Dots and Their Size-Dependent Electrocatalytic Activity for the Oxygen Reduction Reaction. Journal of the American Chemical Society. 2012;134(46):18932-18935.
33. Liu Q, Guo B, Rao Z, Zhang B, Gong JR. Strong Two-Photon-Induced Fluorescence from Photostable, Biocompatible Nitrogen-Doped Graphene Quantum Dots for Cellular and Deep-Tissue Imaging. Nano Lett. 2013;13(6):2436-2441.
34. Peng D, Zhang L, Liang R-P, Qiu J-D. Rapid Detection of Mercury Ions Based on Nitrogen-Doped Graphene Quantum Dots Accelerating Formation of Manganese Porphyrin. ACS Sensors. 2018;3(5):1040-1047.
35. Mihalache I, Radoi A, Pascu R, Romanitan C, Vasile E, Kusko M. Engineering Graphene Quantum Dots for Enhanced Ultraviolet and Visible Light p-Si Nanowire-Based Photodetector. ACS Applied Materials and Interfaces. 2017;9(34):29234-29247.
36. Ganganboina AB, Dutta Chowdhury A, Doong R-a. New Avenue for Appendage of Graphene Quantum Dots on Halloysite Nanotubes as Anode Materials for High Performance Supercapacitors. ACS Sustainable Chemistry and Engineering. 2017;5(6):4930-4940.
37. Tian Z, Yao X, Ma K, Niu X, Grothe J, Xu Q, et al. Metal–Organic Framework/Graphene Quantum Dot Nanoparticles Used for Synergistic Chemo- and Photothermal Therapy. ACS Omega. 2017;2(3):1249-1258.
38. Xie J, Huang K, Yu X, Yang Z, Xiao K, Qiang Y, et al. Enhanced Electronic Properties of SnO_2 via Electron Transfer from Graphene Quantum Dots for Efficient Perovskite Solar Cells. ACS Nano. 2017;11(9):9176-9182.
39. Ramachandran A, J S AN, Karunakaran Yesodha S. Polyaniline-Derived Nitrogen-Doped Graphene Quantum Dots for the Ultratrace Level Electrochemical Detection of Trinitrophenol and the Effective Differentiation of Nitroaromatics: Structure Matters. ACS Sustainable Chemistry and Engineering. 2019;7(7):6732-6743.
40. Ren Q, Ga L, Ai J. Rapid Synthesis of Highly Fluorescent Nitrogen-Doped Graphene Quantum Dots for Effective Detection of Ferric Ions and as Fluorescent Ink. ACS Omega. 2019;4(14):15842-15848.
41. Deming CP, Mercado R, Lu JE, Gadiraju V, Khan M, Chen S. Oxygen Electroreduction Catalyzed by Palladium Nanoparticles Supported on Nitrogen-Doped Graphene Quantum Dots: Impacts of Nitrogen Dopants. ACS Sustainable Chemistry and Engineering. 2016;4(12):6580-6589.
42. Fei H, Ye R, Ye G, Gong Y, Peng Z, Fan X, et al. Boron- and Nitrogen-Doped Graphene Quantum Dots/Graphene Hybrid Nanoplatelets as Efficient Electrocatalysts for Oxygen Reduction. ACS Nano. 2014;8(10):10837-10843.
43. Saidi WA. Oxygen Reduction Electrocatalysis Using N-Doped Graphene Quantum-Dots. The Journal of Physical Chemistry Letters. 2013;4(23):4160-4165.
44. Shen B, Lang J, Guo R, Zhang X, Yan X. Engineering the Electrochemical Capacitive Properties of Microsupercapacitors Based on Graphene Quantum Dots/MnO_2 Using Ionic Liquid Gel Electrolytes. ACS Applied Materials and Interfaces. 2015;7(45):25378-25389.
45. Yan X, Song Y, Zhu C, Song J, Du D, Su X, et al. Graphene Quantum Dot–MnO_2 Nanosheet Based Optical Sensing Platform: A Sensitive Fluorescence "Turn Off–On" Nanosensor for Glutathione Detection and Intracellular Imaging. ACS Applied Materials and Interfaces. 2016;8(34):21990-21996.
46. Shi B, Su Y, Duan Y, Chen S, Zuo W. A nanocomposite prepared from copper(II) and nitrogen-doped graphene quantum dots with peroxidase mimicking properties for chemiluminescent determination of uric acid. Microchimica Acta. 2019;186(7).
47. Liu J, Chen Y, Wang W, Feng J, Liang M, Ma S, et al. "Switch-On" Fluorescent Sensing of Ascorbic Acid in Food Samples Based on Carbon Quantum Dots–MnO_2 Probe. Journal of Agricultural and Food Chemistry. 2015;64(1):371-380.
48. Liu J, Shao J, Wang Y, Li J, Liu H, Wang A, et al. Antimicrobial Activity of Zinc Oxide–Graphene Quantum Dot Nanocomposites: Enhanced Adsorption on Bacterial Cells by Cationic Capping Polymers. ACS Sustainable Chemistry and Engineering. 2019;7(19):16264-16273.
49. Dutta M, Sarkar S, Ghosh T, Basak D. ZnO/Graphene Quantum Dot Solid-State Solar Cell. The Journal of Physical Chemistry C. 2012;116(38):20127-20131.
50. Ebrahimi M, Samadi M, Yousefzadeh S, Soltani M, Rahimi A, Chou T-c, et al. Improved Solar-Driven Photocatalytic Activity of Hybrid Graphene Quantum Dots/ZnO Nanowires: A Direct Z-Scheme Mechanism. ACS Sustainable Chemistry and Engineering. 2016;5(1):367-375.
51. Dhar S, Majumder T, Mondal SP. Graphene Quantum Dot-Sensitized ZnO Nanorod/Polymer Schottky Junction UV Detector with Superior External Quantum Efficiency, Detectivity, and Responsivity. ACS Applied Materials and Interfaces. 2016;8(46):31822-31831.
52. Chen Y-C, Chiang W-H, Kurniawan D, Yeh P-C, Otake K-i, Kung C-W. Impregnation of Graphene Quantum Dots into a Metal–Organic Framework to Render Increased Electrical Conductivity and Activity for Electrochemical Sensing. ACS Applied Materials and Interfaces. 2019;11(38):35319-35326.
53. Teymourinia H, Salavati-Niasari M, Amiri O. Simple synthesis of Cu_2O/GQDs nanocomposite with different morphologies fabricated by tuning the synthesis parameters as novel antibacterial material. Composites Part B: Engineering.

2019;172:785-794.
54. Wang C, Jin J, Sun Y, Yao J, Zhao G, Liu Y. In-situ synthesis and ultrasound enhanced adsorption properties of MoS_2/graphene quantum dot nanocomposite. Chem Eng J. 2017;327:774-782.
55. Ding D, Lan W, Yang Z, Zhao X, Chen Y, Wang J, et al. A simple method for preparing ZnO foam/carbon quantum dots nanocomposite and their photocatalytic applications. Mater Sci Semicond Process. 2016;47:25-31.
56. Jiang R, Zhu H, Yao J, Fu Y, Guan Y. Chitosan hydrogel films as a template for mild biosynthesis of CdS quantum dots with highly efficient photocatalytic activity. Appl Surf Sci. 2012;258(8):3513-3518.
57. Safardoust-Hojaghan H, Salavati-Niasari M. Degradation of methylene blue as a pollutant with N-doped graphene quantum dot/titanium dioxide nanocomposite. Journal of Cleaner Production. 2017;148:31-36.
58. Tauc J, Grigorovici R, Vancu A. Optical Properties and Electronic Structure of Amorphous Germanium. physica status solidi (b). 1966;15(2):627-637.
59. Kumar KV, Porkodi K, Rocha F. Langmuir–Hinshelwood kinetics – A theoretical study. Catal Commun. 2008;9(1):82-84.
60. Largitte L, Pasquier R. A review of the kinetics adsorption models and their application to the adsorption of lead by an activated carbon. Chem Eng Res Des. 2016;109:495-504.
61. Sanchez M, Rivero MJ, Ortiz I. Kinetics of dodecylbenzenesulphonate mineralisation by TiO_2 photocatalysis. Applied Catalysis B: Environmental. 2011;101(3-4):515-521.
62. Kang Z, Liu Y, Tsang CHA, Ma DDD, Fan X, Wong NB, et al. Water-Soluble Silicon Quantum Dots with Wavelength-Tunable Photoluminescence. Adv Mater. 2009;21(6):661-664.
63. Kumar S, Dhiman A, Sudhagar P, Krishnan V. ZnO-graphene quantum dots heterojunctions for natural sunlight-driven photocatalytic environmental remediation. Appl Surf Sci. 2018;447:802-815.
64. Shakeel M, Li B, Arif M, Yasin G, Rehman W, Khan AU, et al. Controlled Synthesis of highly proficient and durable hollow hierarchical heterostructured (Ag-AgBr/HHST): A UV and Visible light active photocatalyst in degradation of organic pollutants. Applied Catalysis B: Environmental. 2018;227:433-445.